energies

MDPI

Article

Passive Islanding Detection of Inverter-Based Resources in a Noisy Environment

Hossein Amini [1], Ali Mehrizi-Sani [1,*] and Reza Noroozian [2]

[1] The Bradley Department of Electrical and Computer Engineering, Virginia Polytechnic Institute and State University, Blacksburg, VA 24061, USA; aminih@vt.edu
[2] Department of Electrical Engineering, University of Zanjan, University Blvd., Zanjan 3879145371, Iran; noroozian@znu.ac.ir
* Correspondence: mehrizi@vt.edu

Abstract: Islanding occurs when a load is energized solely by local generators and can result in frequency and voltage instability, changes in current, and poor power quality. Poor power quality can interrupt industrial operations, damage sensitive electrical equipment, and induce outages upon the resynchronization of the island with the grid. This study proposes an islanding detection method employing a Duffing oscillator to analyze voltage fluctuations at the point of common coupling (PCC) under a high-noise environment. Unlike existing methods, which overlook the noise effect, this paper mitigates noise impact on islanding detection. Power system noise in PCC measurements arises from switching transients, harmonics, grounding issues, voltage sags and swells, electromagnetic interference, and power quality issues that affect islanding detection. Transient events like lightning-induced traveling waves to the PCC can also introduce noise levels exceeding the voltage amplitude by more than seven times, thus disturbing conventional detection techniques. The noise interferes with measurements and increases the nondetection zone (NDZ), causing failed or delayed islanding detection. The Duffing oscillator nonlinear dynamics enable detection capabilities at a high noise level. The proposed method is designed to detect the PCC voltage fluctuations based on the IEEE standard 1547 through the Duffing oscillator. For the voltages beyond the threshold, the Duffing oscillator phase trajectory changes from periodic to chaotic mode and sends an islanded operation command to the inverter. The proposed islanding detection method distinguishes switching transients and faults from an islanded operation. Experimental validation of the method is conducted using a 3.6 kW PV setup.

Keywords: duffing oscillator; grid-following inverters; grid-forming inverters; inverter-based resources; islanding detection; noise; PV system

Citation: Amini, H.; Mehrizi-Sani, A.; Noroozian, R. Passive Islanding Detection of Inverter-Based Resources in a Noisy Environment. *Energies* **2024**, *17*, 4405. https://doi.org/10.3390/en17174405

Academic Editors: Zheng Xu and Salvatore Musumeci

Received: 8 July 2024
Revised: 17 August 2024
Accepted: 30 August 2024
Published: 3 September 2024

1. Introduction

Renewable resources are becoming increasingly popular due to the increasing demand for electricity consumption. This proliferation also introduces new challenges for a power system. For example, islanding poses one of the significant challenges to the safe operation of a power system [1]. Islanding is when a load is supplied by a generator disconnected from the main grid [2]. The combination of the load and the generator is a microgrid. Generally, a microgrid combines generations, lines, and loads working dependently or independently from the main grid.

Islanding can occur either intentionally or unintentionally [3]. In an intentional islanded operation, the goal is to maintain power flow in a part of the grid isolated from the main grid. Some advantages of intentional islanding include facilitating recovery, increasing system reliability, and preventing economic losses. Maintaining an island by distributed generation necessitates fulfilling specific requirements, such as real and reactive power controls, coordination among distributed generations to compensate for island load

fluctuations, voltage control, and synchronization during reconnection. Unintentional islanding occurs when a portion of the grid, due to cyberattacks, faults, protection system errors, or switch failures, separates from the main grid and continues to supply power to the island at a voltage and frequency different from the main grid [4]. Since maintaining the island is not a consideration of the power system design and operation, unintentional islanding can lead to adverse consequences for both the grid and consumers.

Throughout the islanded operation, fluctuations in distributed energy resources (DER) output parameters can cause detrimental effects on the microgrid and the maintenance personnel, ranging from power quality degradation, negative effects on sensitive and important loads, life-threatening for maintenance personnel or residents, severe or slight changes in frequency and voltage, changes in inverter-based resources (IBR) output current [5], asynchronous reclosing, malfunction in protection relays, and the possibility of IBR damaging when the grid returns. Therefore, an accurate islanding detection method is important for the safe operation of a power system and microgrid. From the viewpoint of the IEEE standard 1547, the delay of the open–close mechanism should be the only time available for islanding detection.

During islanded operation, a microgrid can operate in one of the following three ways: the first is to turn off the generations of the microgrid, where the IEEE standard 1547 requires islanding detection and turning off the generations in less than two seconds [6]; the second is the ride-through operation of microgrid generations; the third maintains the islanded microgrid by balancing the generation and the load demand. For each approach, islanding detection is necessary. Islanded operation is indeed detectable using the current measurement of the main circuit breaker. In certain scenarios, when the current passing through the breaker is zero, the detection of islanded operation becomes impossible solely through current measurements. This scenario is when the voltages on two sides of the breaker are the same, and no current passes through the breaker. Most islanding detection methods are proposed to detect islanded operations in such situations. Although it may seem that the most obvious islanding detection method is to monitor the status of switches, the distribution system, unlike the transmission system, does not have a comprehensive data collection system. Such monitoring in the distribution network would require substantial expenditures to establish this system. Therefore, alternative methods are typically employed for islanding detection.

A simple islanding detection method uses conventional frequency and voltage protections [7]. Installing these protections is usually mandatory and is used to maintain the frequency within 1% and the voltage around 10% of the nominal value. If there is a significant imbalance between the real power generated by the distributed generation and the load, the frequency falls outside the desired range, activating the frequency protection. A similar situation may occur for voltage due to reactive power imbalance, causing the voltage protection to activate and disconnect the generation from the grid, thus eliminating the island. While these two protections provide a simple method for detecting and mitigating an islanded operation, problems arise when the imbalances are not large enough to trigger the protections. The island can operate at different but acceptable voltage and frequency levels in such cases. Therefore, other proposed methods have a smaller NDZ and better operational speed.

Islanding detection methods are primarily divided into two categories: remote and local [8]. Remote islanding detection methods are mainly based on communication infrastructures. An example is the power line carrier method. This method sends an islanding signal to the control center once the main circuit breaker is disconnected. Local islanding detection methods are generally categorized into active and passive approaches. Passive islanding detection methods use the point of common coupling (PCC) measurements to detect islanded operation [9]. These methods often have a significant nondetection zone (NDZ) but are easy to implement [10]. Reference [11] proposed an advanced passive islanding detection method for systems incorporating multiple inverters. Reference [12] introduced an index for postprocessing by estimating the number of peaks and valleys within a cycle

using a sliding window, enabling the detection of islanded operation based on the statistical features of the square of the RMS value and the average crest factor. Reference [13] detected islanding based on the cumulative sum of superimposed impedances. Reference [14] introduced a method for islanding detection based on the long short-term memory network. Reference [15] proposed a passive islanding detection method based on the frequency deviations using chaos theory. This study applies a forced Helmholtz oscillator to detect islanded operations for multiple distributed generations.

Active islanding detection methods inject perturbation into the inverter output parameters and detect the islanded operation based on the changes in measurement. The perturbation facilitates islanding detection and decreases the NDZ but causes power quality degradation. Reference [16] employed a small magnitude current injection via α-axis current controller. Reference [17] presented an islanding detection method using a modified active frequency drift. This method proposes a reduced total harmonic distortion without affecting the reliability of the active frequency drift method. Reference [18] incorporated a frequency locked-loop (PLL) that utilizes the voltage phase and frequency at the point of common coupling (PCC), along with a modified auto phase shift (APS), to enable decentralized power generation systems for effective islanding detection. Reference [19] presented a method for islanding detection that leverages the rate of change of kinetic energy and the RMS value of absolute frequency deviation, specifically designed to operate effectively under perfectly matched loading conditions. Hybrid methods combine passive and active islanding detection methods to use their advantages and reduce drawbacks.

The noise effect is neglected in most of the mentioned passive and active islanding detection methods. High ambient noise levels applied to the PCC point measurements can disturb most islanding detection methods. The noise can arise from switching transients, harmonics, grounding issues, voltage sag and swell, electromagnetic interference (EMI), external sources of electromagnetic fields, and power quality issues. For example, a radio frequency (RF) signal, lightning, and the corona effect of a high voltage transmission line can interfere with islanding detection. However, it is important to detect islanded operations in a noisy environment with a small NDZ. The main contribution of this paper is reducing the noise effects on islanding detection. The proposed method utilizes a signal processing approach using a classical Duffing equation to mitigate the impact of noise on islanding detection. The main point of using the Duffing oscillator for islanding detection is that even under a high noise, the Duffing oscillator can discern small periodic signals by altering its phase trajectory from periodic to chaotic mode. The method is tested under different load quality factors and switching events probable for a power system. The proposed method has a negligible NDZ in a high-noise environment, a small detection period, and easy and low-cost implementation. The proposed method is validated in a 3.6 kW PV setup.

Section 2 of this paper presents the study system. Section 3 discusses the application of the Duffing oscillator in weak signal detection and its characteristics on islanding detection, as well as analyzing the proposed method and the noise effect on the islanding detection. Section 4 discusses the simulation and implementation results in grid-connected and islanded operations. Finally, Section 5 concludes the paper.

2. Study System

Figure 1 shows the study system contains a primary source with a voltage-sourced converter (VSC), main grid, and load [7]. The system can work either in grid-connected or islanded modes when the circuit breaker is closed or open, respectively. The primary source and the VSC are connected to the PCC point through a transformer and a series filter which are represented by L_t and R_t in Figure 1. The Thevenin equivalent of the main grid is modeled by a voltage source, the equivalent impedance R_{eq} of the power system, and the equivalent inductance L_{eq} of the lines and loads [20]. The study system parameters are mentioned in Table 1.

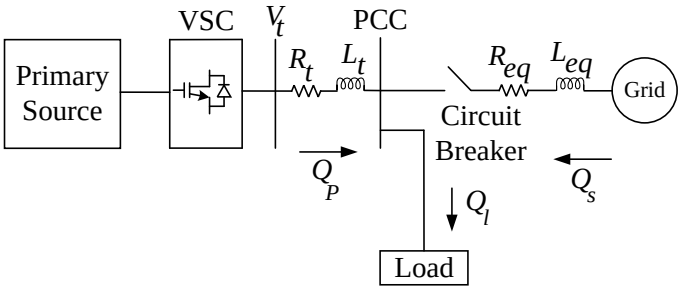

Figure 1. Single line diagram of the study system.

Table 1. Study system parameters.

Inverter and Grid Parameters	Values
L_t	2.3 mH
R_t	5 mΩ
L_{eq}	0.31 mΩ
R_{eq}	12 mΩ
PV output power	100 kW
PV apparent power	120 kVA
DC bus voltage	900 V
f_s	8 kHz
Sampling frequency	16 kHz
V_{L-L}	480 V
f_{Grid}	60 Hz

According to (1), once the load reactive power supplied from the main grid Q_s decreases, the primary source should supply the reactive power shortage of the load Q_l [5]. However, for the islanded operation, Q_s is eliminated from (1), and the primary source should supply the reactive power of the load solely. Thus, a proper islanding system is necessary to control the PCC voltage before and after the islanded operation and to compensate for the load reactive power.

$$Q_l = Q_P + Q_s \tag{1}$$

During a grid-connected operation, an islanding system regulates the output current of the inverter. When the grid is disconnected, the voltage may exceed its threshold [21]. Once the main circuit breaker is disconnected, the PCC voltage must meet the standard criteria. The islanding detection system is responsible for detecting the islanded operation and must modify the grid-following to the grid-forming inverter mode. In the grid-forming inverter mode, the inverter injects the needed reactive power and maintains the PCC voltage in the normal range.

3. Application of the Duffing Oscillator for Weak Signal Detection

The Duffing equation is generally based on the Rayleigh differential Equation (2):

$$\ddot{x} + x + \mu h(x, \dot{x}) = 0, \tag{2}$$

considering $\dot{x}$ as the derivative of x with respect to time, $h(x, \dot{x})$ is a nonlinear expression. If $h(x, \dot{x})$ is chosen as $(x^2 - 1)\dot{x}$, (2) changes to:

$$\ddot{x} + x + \mu(x^2 - 1)\dot{x} = 0. \tag{3}$$

Equation (3) is the van der Pol–Duffing equation. By choosing $\mu = 1$ and $h(x, \dot{x}) = x^3$ the classical Duffing equation is obtained as:

$$\ddot{x} + x + x^3 = 0. \tag{4}$$

Equation (4) is a nonperturbed Duffing equation. By adding $-\xi\dot{x} + \gamma\cos(t)$ to the right side of (4), the perturbed Duffing equation is as follows [22]:

$$\ddot{x} + \xi\dot{x} - \alpha x^3 + x = \gamma\cos(\omega t), \tag{5}$$

which is the general form of a classical Duffing equation. In (5), ξ controls the system damping by dissipating energy and decreasing the amplitude of oscillations over time. The linear stiffness of the system is controlled with α. It measures how the system responds to small displacements from equilibrium. The restoring force nonlinearity is controlled by $-\alpha x^3 + x$, γ is the driving force amplitude, and ω is the angular frequency of the driving force.

The sensitivity of the Duffing oscillator on its initial conditions is used to develop an islanding detection system [23]. The finite cycles in nonlinear systems enable the analysis of state variables through the bifurcation feature [24]. By increasing γ in (5), the period ($\tau = \frac{1}{f}$) of state variables for the Duffing system doubles. For example, it increases from π to 2π or from 2π to 4π. This change in the state of the oscillator is bifurcation. Bifurcation in the Duffing oscillator happens several times, for $\gamma = 0.25$, $\tau = 2\pi$, $\gamma = 0.35$, and $\tau = 4\pi$, and the other bifurcation happens when $\gamma = 0.5$. Increasing $\gamma > 0.7$ causes the state variables of the Duffing oscillator to be in order mode in the time domain. This is the order state of the Duffing oscillator. Increasing $\gamma > 0.83$ changes the Duffing state to chaotic mode. In two- or more-dimensional state spaces, an oscillating response is also one of the possible system responses. The movement of state variables along a closed loop indicates periodic oscillations within the system. When the state trajectory approaches this loop, the system is regarded as stable; otherwise, it is unstable [24]. This paper shows that an islanding event is detectable using the phase plane trajectory of the Duffing oscillator and by changing the state from order to chaos under a high-noise environment.

Equation (5) presents a nonlinear elastic system with the damping ratio γ, nonlinear restoring force $-\alpha x^3 + x$, and the driving force $\gamma\cos(\omega t)$. The nonlinear dynamic system has four modes, and two of the four modes, the order and chaos modes, are used to detect the islanded operation [25]. To investigate the changes on γ, this paper considers $\alpha = 1$ and $\xi = 0.5$ to solve the second-order differential equation using the Runge–Kutta algorithm with a step size of 10^{-5}, which fixes $\gamma_c = 0.83$. Equation (6) is obtained by substituting the constants in (5) considering the PCC voltage and the added noise as the perturbations:

$$\ddot{x} + 0.5\dot{x} - x^3 + x = \gamma\cos(t) + \text{Input voltage} + \varepsilon(t), \tag{6}$$

where $\gamma = \gamma_c$ is the critical point of the Duffing oscillator, and the changes in γ can change the state of the system based on the bifurcation. The frequency of the driving force in (5) under a high-noise environment is equal to the frequency of the signal to be detected. This is characteristic of the Duffing oscillator when the frequency of the driving force is the same as the signal to be detected the Duffing oscillator adds the amplitudes of the driving force to the signal [26]. When the Duffing oscillator is in a critical state, minor changes in system measurements can lead to significant state changes. Increasing γ to values more than γ_c changes the state of the Duffing oscillator from order to chaos. Transitioning from an order to a chaotic state in a high-noise environment changes the coefficients of the fast Fourier transform (FFT) of the Duffing equation output y. FFT coefficients change from symmetrical to unsymmetrical waveforms when γ surpasses γ_c. The even coefficients of the FFT(y) for symmetrical waveforms are almost zero. However, for the unsymmetrical waveforms, the even and odd coefficients of FFT(y) have values other than zeros [27]. Using

FFT(y) for islanding detection, the third and fourth harmonics differences are used as the criteria to send the islanded operation signal to the inverter.

The main difficulty of passive islanding detection methods is determining the threshold. Determining the threshold is important since the detection accuracy depends on the threshold. This paper uses the Melnikov function [23] to calculate the threshold of γ as the amplitude of the driving force [28] for the Duffing oscillator in islanding detection. This function is a predictive tool for nonlinear dynamical systems subjected to periodic perturbations [29]. By analyzing the Melnikov function and identifying when it equals zero, the potential for chaotic dynamics of the Duffing oscillator is revealed subjected to periodic perturbations [30].

$$\begin{aligned} M(t_0) &= \int_{-\infty}^{\infty} \sqrt{2}\,\mathrm{sec}\,h(t)\tanh(t)(\gamma\cos\omega(t+t_0) - \xi y_0(t))dt \\ &= \frac{\sqrt{2}\left(3\pi\cos(\omega)\,\gamma - 2^{\frac{3}{2}}\xi\right)}{3} \end{aligned} \tag{7}$$

To find the threshold, the chaotic state needs to be considered, when $M(t_0) = 0$ and $\xi = 0.5$, then the threshold for γ in (8) is obtained using residue theorem and direct integration [24]:

$$\gamma = \frac{2\cosh(\frac{\pi\omega}{2})}{3\sqrt{2}\pi\omega}. \tag{8}$$

Equation (8) is valid for $\omega = 1$ and $0.37 < \gamma < \gamma_c$. Using this criterion, the amplitudes of the driving force and the signal to be detected add to each other once the driving force and the input signal have small enough frequency differences. The Duffing oscillator can detect a small signal buried in the noise environment if and only if the difference between the frequency of the driving force and the signal to be detected is almost the same ($|\frac{\Delta\omega}{\omega}| \leq 0.03$).

4. Applying Duffing Oscillator to Islanding Detection

Islanding detection using a Duffing oscillator is based on monitoring voltage fluctuations of the PCC. Disconnection of the inverter is necessary for the grid-following inverters when the voltage is outside the normal operating range. Once the main circuit breaker is disconnected, the islanding system should change the operation strategy from grid-connected to islanded mode. Using a grid-forming inverter, the inverter continues to operate in island mode when the main circuit breaker is disconnected from the main grid and during islanded operation. The grid-forming inverter maintains the voltage and frequency of the island and stabilizes the island for resynchronization [21]. Considering a PV system as the primary source, the injected power from the PV system is $P_{PV} + jQ_{PV}$, and the difference in power supplied from the main grid is $\Delta P + j\Delta Q$.

The protection mechanism detects an islanded operation through voltage deviations beyond the standard range. Following the IEEE standard 1547, the voltage range in a grid-connected operation is between 88% and 110% of the nominal voltage. Table 2 represents the response of DER to abnormal voltage conditions of a power system [6]. This table guides the appropriate setting of DER trip functions in response to abnormal voltage conditions, promoting the reliability and security of the grid [6]. In this table, OV reflects the overvoltage and UV reflects the undervoltage limits.

Table 2. DER response to abnormal voltages.

Shall Trip Function	Voltage (pu)	Clearing Time (s)
OV2	fixed at 1.20	fixed at 0.16
OV1	1.10–1.20	1.00–13.00
UV1	0.00–0.88	2.00–21.00
UV2	0.00–0.50	0.16–2.00

Three different conditions are probable for islanding detection using the Duffing oscillator. The first condition is when the output reactive power of the PV is equivalent to the power demand of the load. In this condition, the Duffing oscillator is accompanied by the rate of change of voltage (ROCOV) for islanding detection. Differentiating the voltage variations using ROCOV magnifies the smallest changes and facilitates the islanding detection [31]. In the second condition, the reactive power is injected from the grid into the local load ($\Delta Q_s > 0$), whereby the PCC voltage is lower than the grid voltage during the islanded operation. In the third scenario, reactive power is injected from the local load into the grid ($\Delta Q_s < 0$), where the PCC voltage is greater than the grid voltage during islanded operation.

4.1. Analysis of the Proposed Method

In (5), the driving force frequency is ω rad/s. The normal frequency of the grid is 60 Hz. The grid dynamics, including load and generation changes, change the normal operation frequency based on Table 3 [6]. The Duffing equation frequency for islanding detection should be compatible with the normal frequency range of the main grid. This normal frequency is not necessarily limited to 60 Hz. To match the grid frequency with the Duffing oscillator driving force frequency, an array of Duffing oscillators is used in this paper to cover the whole normal frequency domain of a 60 Hz power system.

Table 3. DER response to abnormal frequencies.

Shall Trip Function	Frequency (Hz)	Clearing Time (s)
OF2	62.00	0.16
OF1	61.20	300.00
UF1	58.50	300.00
UF2	56.50	0.16

Based on Table 3, to ensure the synchronous operation of the detection system with the grid frequency, it is imperative to set a specific driving force frequency range for the Duffing array between 58.5 Hz and 61.2 Hz. A frequency transformation of the Duffing equation driving force is indispensable to achieve this requisite frequency alignment. This transformation is realized by substituting a time variable, t, related to ω via the equation $t = \omega\tau$ and considering $\omega = 2\pi f$:

$$\begin{cases} x(t) = x(2\pi f\tau) \\ \dot{x}(t) = \frac{1}{2\pi f}\frac{dx(2\pi f\tau)}{d\tau} \\ \ddot{x}(t) = \frac{1}{(2\pi f)^2}\frac{dx^2(2\pi f\tau)}{d\tau^2}, \end{cases} \tag{9}$$

by substituting (9) in (6), (10) is obtained as:

$$\frac{1}{(2\pi f)^2}\frac{dx^2(2\pi f\tau)}{d\tau^2} + \frac{0.5}{2\pi f}\frac{dx(2\pi f\tau)}{d\tau} - x^3(2\pi f\tau) + x(2\pi f\tau) = \gamma\cos(2\pi f\tau) \tag{10}$$

Equation (10) is used to synchronize the islanding detection method with a power system that works in f normal operation frequency [28].

4.2. Noise Effect on the Proposed Islanding Detection Method

In this paper, the noise is considered as an additional input. The dynamics of the system are described in terms of the state variables x and y, and the input is added to the system in (11):

$$\begin{cases} \dot{x} = \omega y \\ \dot{y} = \omega(-0.5y + x^3 - x + \gamma\cos(\omega\tau) + \delta\cos((\omega + \Delta\omega)\tau + \varphi) + \varepsilon(t)), \end{cases} \tag{11}$$

where $\varepsilon(t)$ is the Gaussian white noise with the root mean square σ, $\Delta\omega$ is the small enough frequency difference between the driving force and the voltage signal, where $\Delta\omega \ll \omega$, and φ is the primary phase difference between the driving force and voltage signal. The above transformation led to the construction of the Duffing oscillator array to detect islanded operations in the normal frequency range. This array comprises several uncoupled Duffing oscillators with different frequency definitions. In this array, each Duffing oscillator is responsible for islanding detecting in a very narrow frequency extent $\Delta\omega$ [32]. The Runge–Kutta algorithm is sensitive to the different step sizes, and there is a truncation (discretization) error when using the Runge–Kutta algorithm due to the infinite Taylor series. The truncation error causes a distinct discrepancy of the critical value γ_c for different step sizes. Changing the step size in numerical simulations does not result in a phase trajectory transition. The only parameter that changes the phase trajectory is γ_c. For the Duffing oscillator, the phase transition happens if and only if the frequency of the voltage signal and the driving force are close enough ($|\frac{\Delta\omega}{\omega}| \leq 0.03$). The total periodic force of the Duffing oscillator containing the driving force, the PCC voltage, and the ambient noise is obtained using (6) as:

$$\begin{aligned}\text{Total Amplitude} = \gamma_c \cos(\omega\tau) + \delta\cos((\omega+\Delta\omega)\tau+\varphi) = \gamma_c\cos(\omega\tau) + \delta\cos(\omega\tau)\\ \cos(\Delta\omega\tau+\varphi) - \delta\sin(\omega\tau)\sin(\Delta\omega\tau+\varphi).\end{aligned} \tag{12}$$

Assuming the total amplitude in (12) is equal to the $A(\tau)\cos(\omega\tau+\varphi_t(\tau))$, then $A(\tau)$ and $\varphi_t(\tau)$ are achievable using (13) and (14), respectively, [32] as follows:

$$A^2(\tau) = (\gamma_c)^2 + 2\gamma_c\delta\cos(\Delta\omega\tau+\varphi) + \delta^2 \tag{13}$$

and

$$\gamma_c\sin(\varphi_t(\tau)) = \delta\cos(\varphi_t(\tau))\sin(\Delta\omega t+\varphi) - \delta\sin(\varphi_\tau(\tau))\cos(\Delta\omega\tau+\varphi). \tag{14}$$

In (13) and (14), there are three probabilities for the Duffing oscillator state. If $\Delta\omega$ is negligible, then $A = \sqrt{{\gamma_c}^2 + 2\gamma_c\delta\cos(\varphi)+\delta^2}$ and the phase difference (φ) can change the state of the Duffing oscillator. For $\pi - cos^{-1}(\frac{\delta}{2\gamma_c}) \leq \varphi \leq \pi + cos^{-1}(\frac{\delta}{2\gamma_c})$, when $\gamma \leq \gamma_c$ the Duffing oscillator remains in its initial state (order mode) [33]. When φ is not in this range, the Duffing oscillator cannot detect the islanded operation correctly. In this paper, the driving force amplitude is considered to be half of the voltage amplitude in normal operation. This consideration causes a negligible NDZ resulting from φ. For a significant $\Delta\omega$, when $A(\tau) = \gamma_c + \delta$, the Duffing oscillator is in its chaotic mode, and for $A(\tau) = \gamma_c - \delta$, it is in its order mode. A feedback loop assesses the number of chaotic Duffing oscillators in the array. The frequency of the Duffing oscillator is calculated using $f_\Delta = \frac{\Delta\omega}{2\pi}$ and checked with the grid frequency. For a significant $\Delta\omega$, the $\varphi(\tau)$ effect is negligible on islanding detection.

4.3. Noise Immunity of the Islanding Detection Method

In this study, the power of the noise is increased gradually to check when the proposed method cannot detect the islanded operation through the noise. This point is considered the worst-case signal-to-noise ratio for the proposed method. The noise in this study is the measuring point noise. The power system is considered to work in a remote place such that the noise cannot affect the power system stability. The SNR value represents that for 1 pu of the voltage, the maximum noise amplitude in measurement should not exceed eight times bigger than the voltage signal. However, the proposed method can detect islanded operation in a real power system when the signal-to-noise ratio in PCC is not exceeded by:

$$\text{SNR} = 20\log(\frac{V^2}{4\sigma^2}) = 7.04\ \text{dB}. \tag{15}$$

The simulation and experimental results show that the proposed islanding detection method detects an islanded operation in an environment with about 7.04 dB signal-to-noise ratio in reality. The noise amplitude is almost three times smaller than a power system voltage signal amplitude in this ratio.

5. Simulation and Experimental Results

Based on the two different probabilities for the voltage amplitude and ambient noise, this paper considers a weaker noise power compared to the voltage amplitude. Figure 2 shows the proposed system used to validate the proposed islanding detection method.

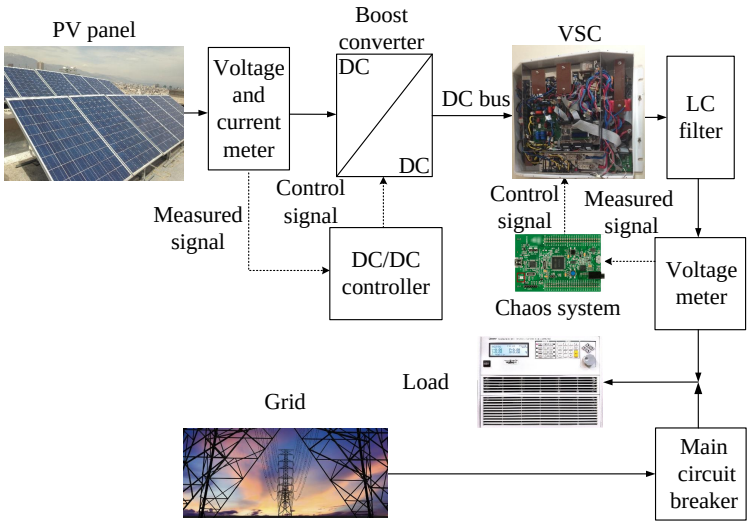

Figure 2. The block diagram of the study system and the proposed islanding detection method.

5.1. Case 1: Normal Operation before Islanding

Figure 3 shows the flowchart of the proposed islanding detection method. In this flowchart, the criteria are based on the IEEE standard 1547, and the measured voltage at the first level should meet the normal criterion $88\% < V \leq 110\%$. If the first criterion is not met, the second criterion checks whether the voltage is in the $50\% \leq V \leq 88\%$ or $110\% \leq V \leq 120\%$. If the PCC voltage violates the second criterion for $t_{dl} > 1$ s, the system should be checked for islanded operation using the Duffing oscillator. In this flowchart, t_{dl} is the delay time that the islanding detection algorithm is not activated. For the defeated criteria for more than the t_{dl}, islanding detection checks the islanded operation. The last criterion is $V < 50\%$ or $V > 120\%$ in Table 2, and if the voltage limit beyond the criterion lasts $t_{dl} > 2$ s, the system should be checked for islanded operation. The FFT of the output signal of the Duffing oscillator is then calculated, and the difference between the third and fourth harmonics should not exceed 0.12 for normal operation. The islanded operation signal is sent to the inverter if this criterion is defeated. To consider the switching transients, a $t_{dl} > 0.4$ s delay is applied to the detection system before deciding on the islanded operation.

For the noise with a root mean square of $\sigma = 0.21$ and the SNR = 25 dB, the phase plane trajectory of the Duffing oscillator for simulation result with $|\frac{\Delta\omega}{\omega}| = 0$ and $\varphi = \pi/3$ is shown in Figure 4a in simulation and Figure 4b in implementation. The phase plane trajectory of the Duffing oscillator is in its periodic state, and no state transition occurs since the PCC voltage is in its normal operation. For $|\frac{\Delta\omega}{\omega}| \leq 0.03$, the experimental results are the same as the theoretical results. That is, for $|\frac{\Delta\omega}{\omega}| > 0.03$, the phase transition due to quick changes of $\gamma(t)$ is not reliable. $\sigma = 0.05$ and SNR = 1 dB are considered for the weak noise and a considerable voltage signal scenario as the second probability, which is not sensible in real power system islanding studies.

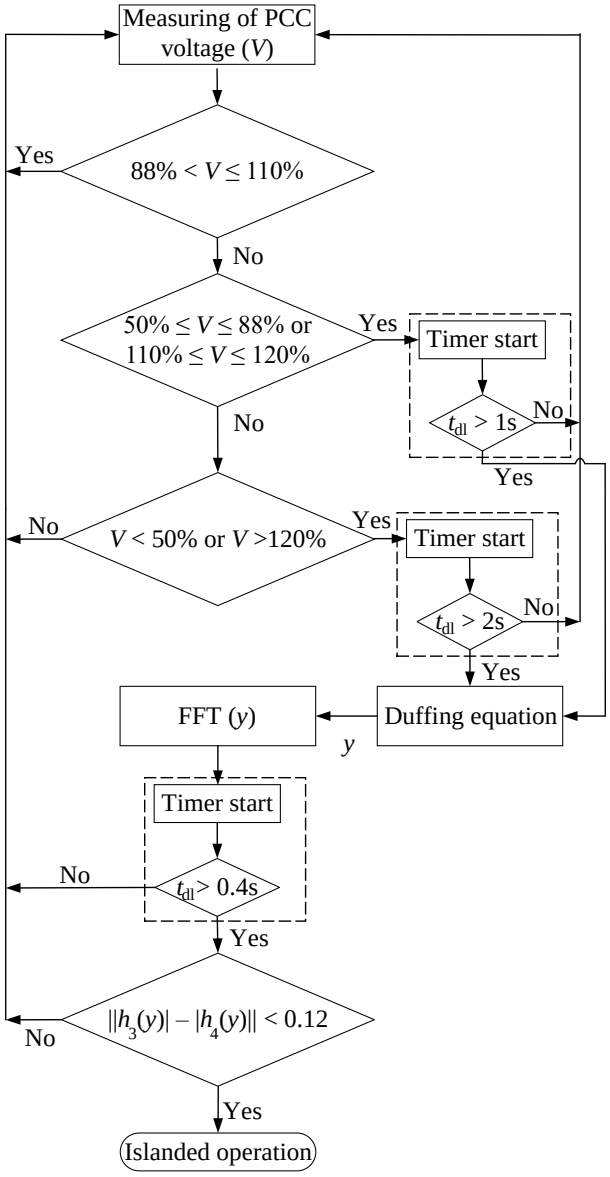

Figure 3. Flowchart of the proposed islanding detection method using the Duffing equation.

Transition in the phase plane trajectory of the Duffing oscillator happens if and only if the driving force frequency is close enough to the voltage signal. Thus, an array of Duffing oscillators is needed for islanding detection with a voltage signal and weak noise, which is more probable in power system operations. In the simulation and the implementation results, $58.5 \leq f \leq 61.2$ is the normal frequency range of the power system. Figure 5 shows the implementation testbed. ARM microcontroller is programmed to process the Duffing equation with the input perturbations, including noise and PCC voltage. A transformer is connected to the PCC point, and a voltage divider with an offset provider, Opamp, is used to change the voltage level for processing in the ARM microcontroller. It is worth noting that the internal inverter digital signal processing (DSP) could also be used instead of the ARM microcontroller in the testbed. The only considerations for the DSP are the digital-to-analog (D/A) and analog-to-digital (A/D) converters that are not embedded in some of the DSP modules.

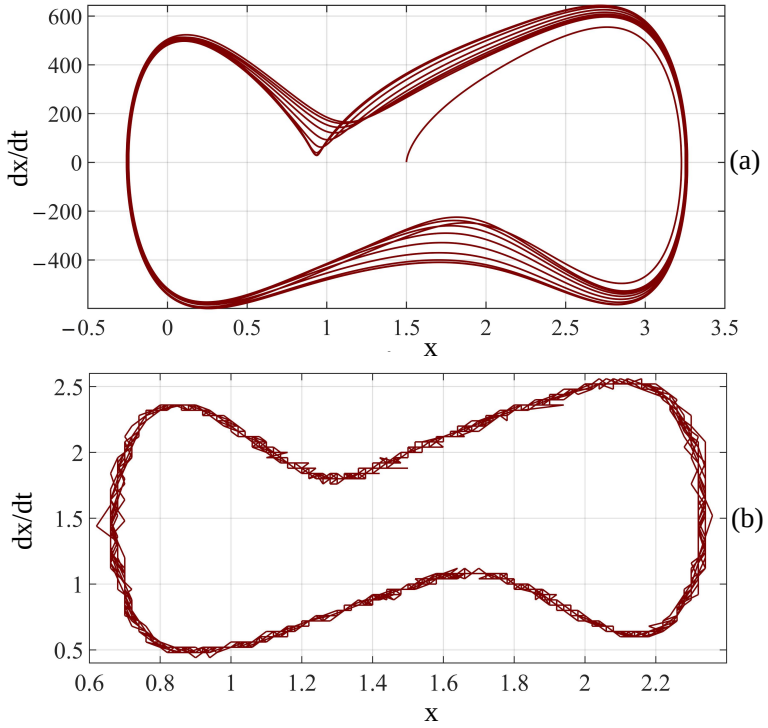

Figure 4. Phase trajectory of the Duffing oscillator for the voltage signal and the noise with $\sigma = 0.21$ and the SNR = 25 dB: (**a**) simulation; (**b**) implementation.

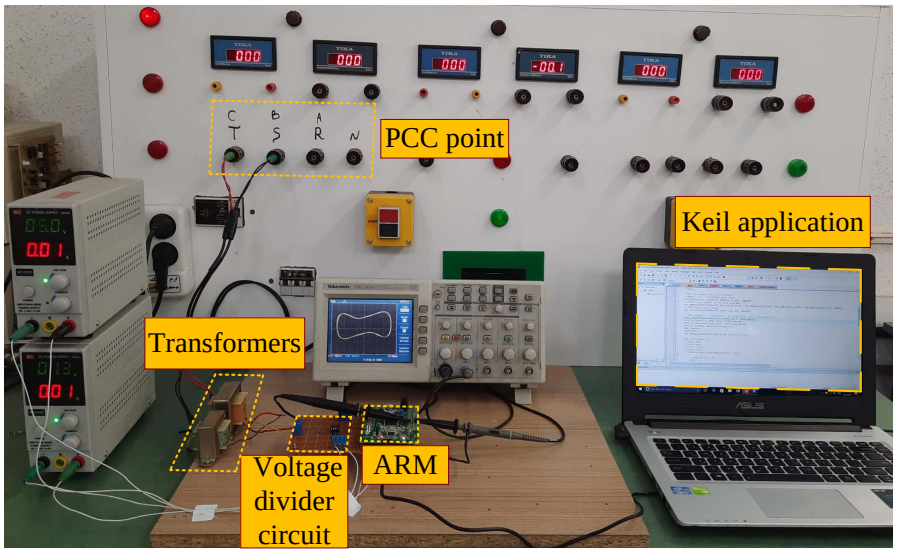

Figure 5. Experimental setup for islanding detection using Duffing oscillator.

The ARM microcontroller processes real-time voltage deviations from the threshold in the Duffing equation for islanding detection. A voltage reduction is needed to utilize the STM32f407Discovery ARM microcontroller to implement the proposed method on the 3.6 kW PV setup. It is essential to ensure that the input voltage of the ARM microcontroller is converted to its appropriate voltage range. The voltage reduction process must be accompanied by physical isolation between the PCC and the ARM to prevent physical damage during faults. The transformer ensures a safe voltage reduction with mechanical and electrical isolations, and the resistive divider after the transformer ensures the proper voltage range for the ARM microcontroller. An OP07CP Opamp with a 1.5 V offset is used to compatible the voltage signal with the ARM input voltage range. Figure 6 shows the

transformer, resisters, Opamp circuit, and the ARM microcontroller programmed by Keil μversion 5 to perform the Duffing equation in the normal and islanded operation of the system. Figure 7a in simulation and Figure 7b in implementation shows the phase plane trajectory of the Duffing output in grid-connected operation mode.

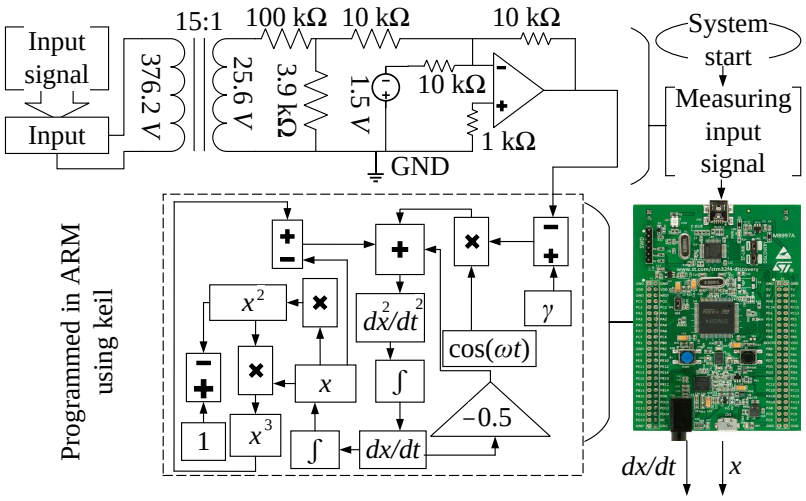

Figure 6. Detailed step-down voltage circuit for the ARM microcontroller.

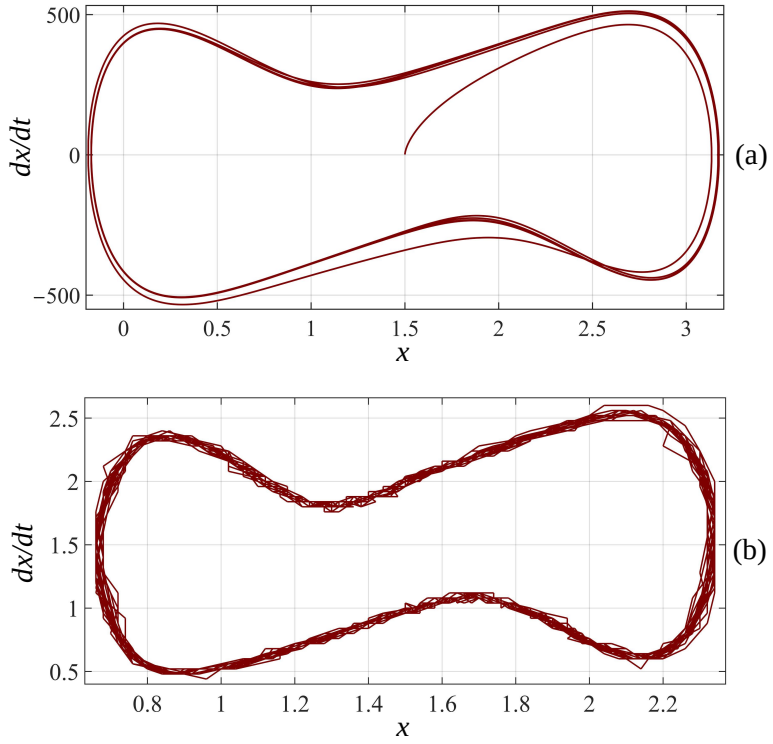

Figure 7. The Duffing oscillator phase trajectory in order mode at the normal operation of the system: (**a**) simulation; (**b**) implementation.

5.2. Case 2: Islanded Operation

For islanded operation, t = 0.2 s in simulation, the main circuit breaker disconnects the grid. The PCC voltage increases significantly since loads are mostly inductive in a real grid. Consider the probability of the voltage signal having a larger amplitude than the noise signal. For the islanded detection, an array of oscillators with different frequencies between 58.5 and 61.2, with a 0.03 difference, is needed for 90 Duffing oscillators. All these oscillators are integrated within a single ARM microcontroller. The Duffing oscillator detects weak signals among noise based on the similarity between the frequency of the driving force and the signal to be detected. The Duffing oscillator can detect the voltage signal among noise when the voltage frequency signal from the driving force frequency is less than 0.03 Hz. The Duffing oscillator array is considered as $\Omega = [\omega_1, \omega_2, \cdots, \omega_{90}]$. This array is an equal-ratio array made up of the 90 Duffing oscillators with:

$$f_1 = 58.50, f_2 = 58.53, \cdots, f_{90} = 61.20. \tag{16}$$

The difference between the third and the fourth coefficients of the FFT, which is calculated using the Duffing oscillator output, is considered the criteria for the islanded signal. When islanding occurs, for 58.5 Hz $< f <$ 61.2 Hz, the regular intermittent chaos happens in two adjacent Duffing oscillators (n and $n + 1$). The equivalent frequencies for these two oscillators are f_n and f_{n+1}. In these two frequencies, the phase plane trajectories of the Duffing oscillators change from order to chaos states. The even coefficients of the FFT(y) (y is the output signal of the Duffing oscillator) change from almost 0 to almost 1. Since the coefficients are not exactly 0 and 1, the islanding command signal is sent to the inverter if and only if $||h_3| - |h_4|| > 0.12$, where $|h_3|$ is the absolute value of the third harmonic extracted from the FFT(y) and $|h_4|$ is the absolute value of the fourth harmonic. The series filter used in the system, as shown in Figure 1, is designed to mitigate high-frequency noise and harmonics, ensuring the system operation. The noise referred to in this article is the PCC measurement noise. The filter is designed to mitigate the harmonics of the PCC voltage caused by inverter switching. For the third and fourth harmonics, the filter can effectively reduce noise and ensure clean signal input to the PCC. However, for other types of harmonics and high-frequency noise, the filter capability cannot affect the accuracy and response time of the islanding detection method, since the driving force frequency of the Duffing oscillator is highly sensitive to the frequency of the signal to be detected. A time delay of 0.4 s is considered for the proposed islanding detection method to eliminate the load-switching effect. The phase plane trajectory of Figure 8a represents the chaos mode of the Duffing oscillator in simulation, and Figure 8c shows the chaos mode of the Duffing oscillator in implementation. Figure 8b shows the time and velocity diagrams of the islanded mode in simulation, and Figure 8d in implementation. In this mode, the islanding system sends the islanded operation signal to the inverter, and the grid-following inverter changes its mode to grid-forming to stabilize the island by dampening the fluctuations.

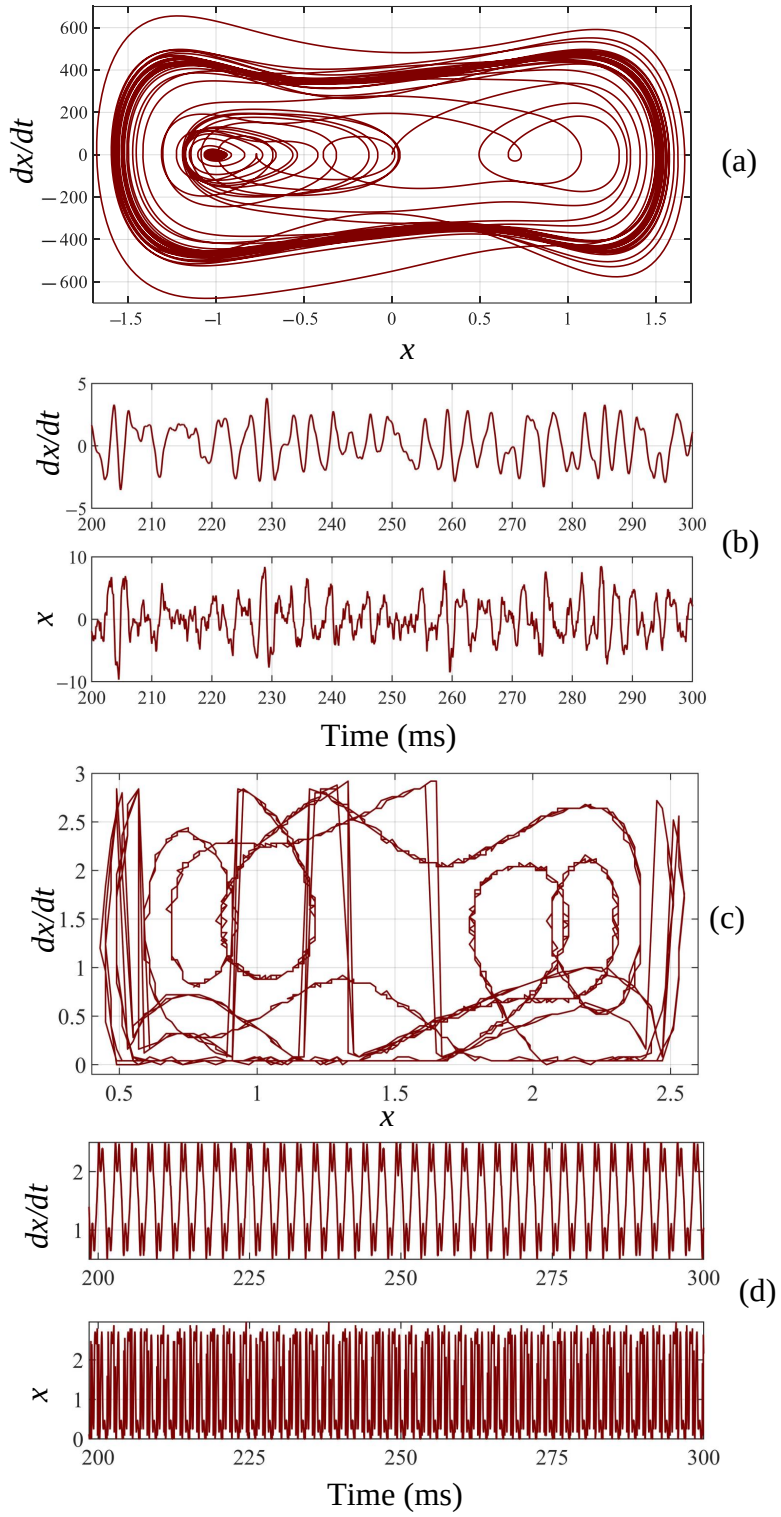

Figure 8. Islanded operation of the system: (**a**) chaos phase trajectory of the Duffing oscillator in simulation, (**b**) $x - t$ and $\frac{dx}{dt} - t$ diagrams in simulation, (**c**) chaos phase trajectory of the Duffing oscillator in implementation, and (**d**) $x - t$ and $\frac{dx}{dt} - t$ diagrams in implementation.

5.3. Case 3: Normal Operation after Islanding

When the islanded inverter is reconnected to the grid at t = 0.4 s, the voltage returns to its steady state after minor fluctuations (0.1 s). During this transition, the phase plane

trajectory of the detection system shifts from chaos to order mode. The time response of the transient process is less than 1 cycle, which meets the IEEE standard 1547 criteria. Once the main circuit breaker is reconnected, the detection system returns to its normal state after a transient period.

Figure 9a,b show the $x - t$ and $\frac{dx}{dt} - t$ diagrams in the normal operation of the system after the transient period in simulation and implementation, respectively. The power cutoff time is 0.2 s and the reconnection time is 0.4 s. In this paper, the criteria for islanding detection are based on the UL 1741 test [34]. This test specifies that the method for islanding detection must successfully detect islanded operation for an *RLC* load with $Q_f \leq 1.8$ within 2 s. This paper considers system switching and inverter switching as the switching events. These switching events last up to 10^{-1} s. The proposed method should distinguish the islanding operation from faults or switching events properly. This method is valid for islanding detection in various quality factors, load-switching conditions, and load imbalance situations.

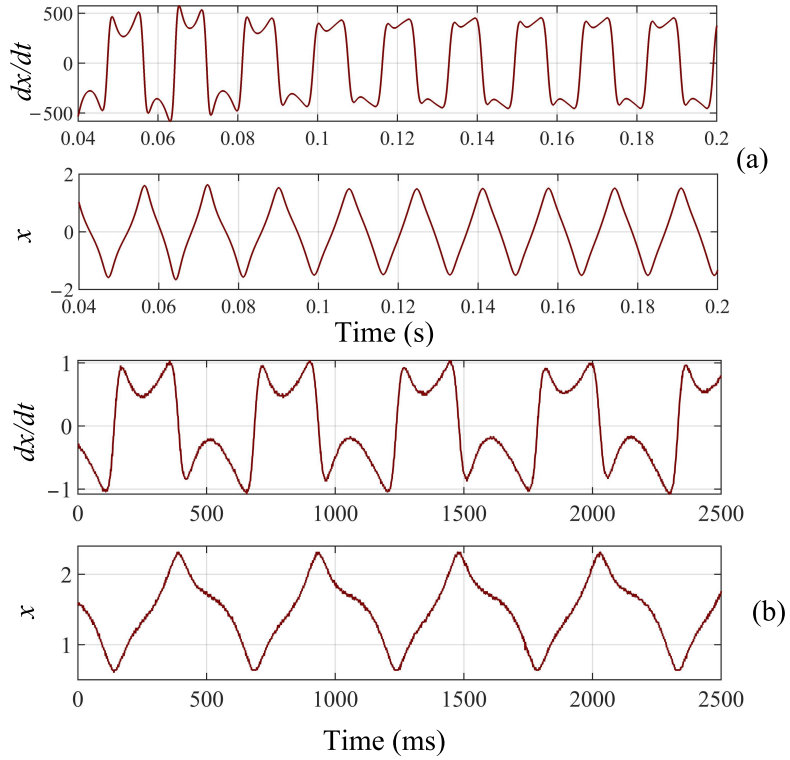

Figure 9. $x - t$ and $\frac{dx}{dt} - t$ diagrams of the Duffing oscillator in grid-connected operation: (**a**) simulation; (**b**) implementation.

5.4. Case 4: Normal Operation with Noise Interference

Figure 10 shows the PCC voltage interfered with noise. The noise signal in this figure distorts the voltage signal and the phase trajectory both in simulation and implementation. The noise cannot alter the Duffing oscillator mode when SNR = 10 dB. Figure 10a shows the noise applied to the voltage signal for the SNR in the Duffing oscillator detection range. Figure 10b is the distorted voltage signal with noise, which is less than the Duffing oscillator detection limit. Figure 10c shows that the noise can distort the phase trajectory without affecting the detection process. Figure 10d is the phase trajectory output of the Duffing oscillator in implementation. It is mentioned that the noise power beyond the Duffing oscillator SNR tolerance can devastate the phase plane trajectory, leading to detection failure. The maximum noise tolerance of this method for islanding detection is obtained using the SNR criterion.

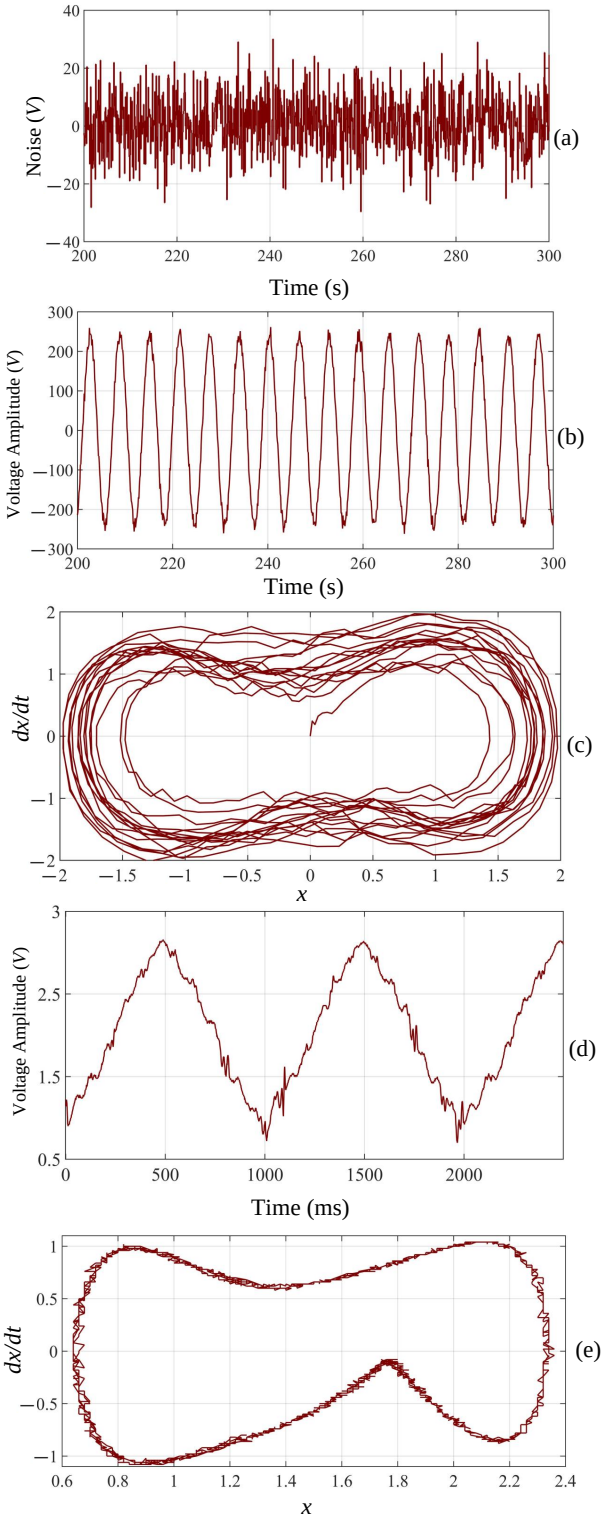

Figure 10. Noise effect on the proposed islanding detection method: (**a**) the noise signal in simulation, (**b**) distorted voltage signal with noise in simulation, (**c**) phase trajectory of the Duffing oscillator in order mode and normal operation of the system under the noise in simulation, (**d**) distorted voltage signal with noise in implementation, and (**e**) order mode of the phase trajectory for the Duffing oscillator in normal operation of the system under distorted voltage with the noise in implementation.

6. Performance Evaluation of the Proposed Islanding Detection Method

Islanding detection methods are evaluated and compared according to several key criteria. These include compatibility with the type of primary energy source, implementation costs, suitability for systems with multiple distributed generators (DG), impact on power quality, the nondetection zone, type of load, quality factor, response time, and vulnerability to cyberattacks.

The proposed islanding detection method is applicable to both inverter-based resources and synchronous generators. However, it is not suitable for systems with multiple DG. A significant advantage of this method is that it does not introduce any disturbances to the power quality of the system and has very low implementation costs. While it is suitable for various load types, capacitive loads affect its performance. According to the UL1741 test [34], the most challenging scenario for detecting islanded operations occurs when $Q_{load} \leq 1.8$. The proposed method is capable of detecting islanded operations in this condition and generates an islanding signal. However, it is vulnerable to cyberattacks, and incorporating encryption and decryption mechanisms could improve its resilience against such threats.

6.1. Response Time of the Proposed Islanding Detection Method

Given the detrimental effects of islanded operations on a microgrid, reducing the detection response time is of critical importance. This section compares the response time of the proposed islanding detection method with passive islanding detection methods in Table 4 [35].

Table 4. Response time of the passive islanding detection methods.

Passive Methods	**Response Time**
Rate of Change of Frequency over Power	100 ms
Rate of Change of Frequency (ROCOF)	24 ms
Phase Jump Detection	10–20 ms
Rate of Change of Active and Reactive Power	24–26 ms
Total Harmonic Distortion	45 ms
Over Under Voltage/Over Under Frequency	4 ms–2 s
Signal Processing Methods	Response Time
Discrete Fourier Transformation	1 ms
Continuous wavelet Transformer	0.6 s
S-Transformer	26–28 ms
Time-Time Transformer	25 s
Kalman Filter	50–70 ms
Hilbert Huang transform	Less than 2 cycle
Intelligent Methods	Response Time
Artificial Neural Network (ANN)	0.2 s
Phase-space technique	0.24 s
Signal energy using Wavelet	32 ms
$Q - Q_{inv}$ Fuzzy logic	0.68 s
Adaptive Neuro-Fuzzy Inference System	0.062 s
Voltage and current RMS	0.040 s
Naive Bayesian classifier	0.12 s
The proposed Method	Response Time
Proposed Islanding Detection Method	556 ms

6.2. Nondetection Zone of the Islanding Detection Method

NDZ presents a range of conditions or situations where an islanding detection method cannot recognize the islanded operation [36]. Decreasing NDZ is important to ensure the reliability of the islanding detection method. This paper uses the real and reactive power

mismatches to calculate NDZ [37]. For an RLC load, the reactive power of the load is calculated as follows [31]:

$$Q = \frac{3V^2}{\omega_n L} - 3V^2\omega_n C. \tag{17}$$

For the grid-connected operation mode of the inverter and considering a unity power factor, the load reactive power equals the reactive power mismatch [31]:

$$\Delta Q = \frac{3V^2}{\omega_n L}(1 - \omega_n^2 LC) = \frac{3V^2}{\omega_n L}(1 - \frac{\omega_n^2}{\omega_r^2}). \tag{18}$$

Considering $\omega_r = \omega_n \pm \Delta\omega$, the reactive power mismatch is obtained as follows:

$$\Delta Q = \frac{3V^2}{\omega_n L}(1 - \frac{f_n^2}{(f_n \pm \Delta f)^2}), \tag{19}$$

where ω_n is the load nominal frequency, L is the load inductance, R is the load resistance, V is the voltage, and Δf is the frequency range based on the IEEE standard 1547. Real power mismatch is similarly calculated as [38]:

$$\Delta P = \pm 3V\Delta VI = \frac{3V^2}{R}(1 - \frac{1}{(1 \pm \Delta V)^2}). \tag{20}$$

Figure 11 shows that the NDZ of the proposed method is smaller than the other references, which can acknowledge the reliability of the islanding detection method. Simulations show that when L_{eq} is varied between 0.1 and 0.5 pu, a stiff grid (SCR > 5), the proposed method remains robust. The method tolerates variations of up to ±10% in L_t and L_{eq} without significant performance degradation. This demonstrates the resilience of the proposed method under real-world conditions. Under weak grid conditions, however, the system becomes unstable.

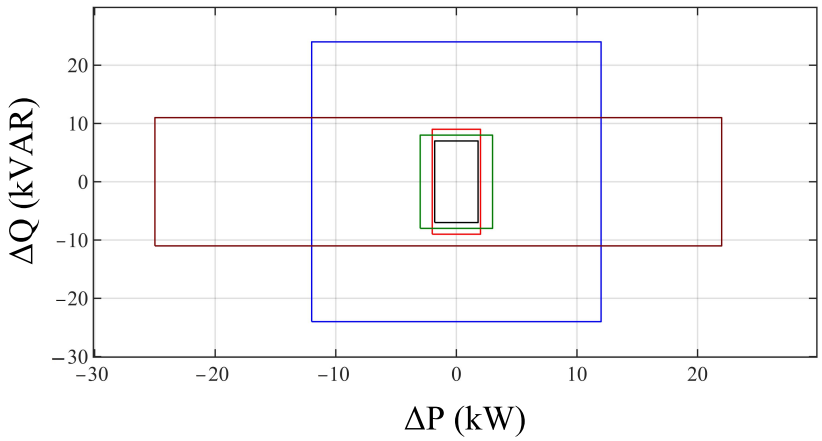

Figure 11. NDZ comparison of the proposed islanding detection method with the passive islanding detection methods. Crimson represents the NDZ for [16], blue for [18], green for [7], red for [31], and black denotes the NDZ for the proposed method.

7. Conclusions

This paper proposed a passive islanding detection method using chaos theory based on a classical Duffing oscillator. The method can detect islanded operations using a signal processing method in a high-noise environment. The basic idea of the method is to detect a weak signal by changing the phase plane trajectory of the Duffing oscillator from order to chaos by changing the coefficients of the Duffing output FFT. The simulation results are carried out in MATLAB and validated in a 3.6 kW PV setup. The results show that

the proposed method is reliable, accurate, and does not interfere with power quality, making it a suitable solution for islanding detection under a high-noise environment. The primary limitation of the chaos method under consideration pertains to its inability to detect islanding events where there is no discernible difference between the primary source output power operating in island mode and the local load power demand, which is addressed in this paper using the ROCOV method. Moreover, simulations confirm that the proposed method remains robust under stiff grid conditions, but may require further adjustment for weak grid scenarios. For future work, an investigation of different noise levels and a thorough investigation of noise effects on the islanding detection method is valuable. This analysis includes various noise scenarios, such as high-frequency noise, harmonic distortion, and random disturbances, to assess how these factors influence the accuracy and reliability of the detection process. Studying these effects in detail provides a more comprehensive evaluation of the method performance in real-world applications.

Author Contributions: All authors conceptualized the work. H.A. performed writing, analysis, and material gathering. A.M.-S. completed the writing, reviewing, and editing of the work. R.N. edited and revised the work. All authors have read and agreed to the published version of the manuscript.

Funding: This work is supported in part by the National Science Foundation (NSF) under award ECCS-1953213, in part by the State of Virginia's Commonwealth Cyber Initiative (www.cyberinitiative.org), in part by the U.S. Department of Energy's Office of Energy Efficiency and Renewable Energy (EERE) under the Solar Energy Technologies Office Award Number 38637 (UNIFI Consortium led by NREL), and in part by Manitoba Hydro International. The views expressed herein do not necessarily represent the views of the U.S. Department of Energy or the United States Government.

Data Availability Statement: Not Applicable.

Conflicts of Interest: The authors declare no conflicts of interest.

References

1. Saleh, K.A.; Mehrizi-Sani, A. Harmonic Directional Overcurrent Relay For Islanded Microgrids with Inverter-Based DGs. *IEEE Syst. J.* **2021**, *15*, 2720–2731. [CrossRef]
2. Syed, M.; Mehrizi-Sani, A.; Robowska, M.; Guillo-Sansano, E.; Wang, D.; Burt, G. Dynamically robust coordinated set point tracking of distributed DERs at point of common coupling. *Int. J. Electr. Power Energy Syst.* **2022**, *143*, 108481. [CrossRef]
3. Pavankumar, Y.; Debnath, S.; Paul, S. A New Lissajous-Based Technique for Islanding Detection in Microgrid. *IEEE Trans. Smart Grid* **2024**, *15*, 2856–2865. [CrossRef]
4. Chen, L.; Dong, X.; Wang, B.; Shang, L.; Liu, C. An Edge Computing-Oriented Islanding Detection Using Differential Entropy and Multi-Support Vector Machines. *IEEE Trans. Smart Grid* **2024**, *15*, 191–202. [CrossRef]
5. Saleki, A.; Bina, M.T.; Shahirinia, A. Suggesting Hybrid HB and Three-Quarter-Bridge MMC-Based HVDC Systems: Protection and Synchronous Stability Under DC Faults. *IEEE Trans. Power Deliv.* **2022**, *37*, 2693–2703. [CrossRef]
6. *IEEE Std 1547-2018 (Revision of IEEE Std 1547-2003)*; IEEE Standard for Interconnection and Interoperability of Distributed Energy Resources with Associated Electric Power Systems Interfaces. IEEE: Piscataway, NJ, USA, 2001.
7. De, S.; Reddy, M.V.; Sodhi, R. A Data-Driven Passive Islanding Detection Scheme. *IEEE Trans. Ind. Appl.* **2024**, *60*, 3698–3709. [CrossRef]
8. Cebollero, J.A.; Cañete, D.; Martín-Arroyo, S.; García-Gracia, M.; Leite, H. A survey of islanding detection methods for microgrids and assessment of non-detection zones in comparison with grid codes. *Energies* **2022**, *15*, 460. [CrossRef]
9. Liu, Y.; Mili, L.; Xu, Y.; Zhao, J.; Kamwa, I.; Srinivasan, D.; Mehrizi-Sani, A.; Arboleya, P.; Terzija, V. Guest editorial: Special issue on data-analytics for stability analysis, control, and situational awareness of power system with high-penetration of renewable energy. *Int. J. Electr. Power Energy Syst.* **2022**, *137*, 107773. [CrossRef]
10. Abu Sarhan, M. An Extensive Review and Analysis of Islanding Detection Techniques in DG Systems Connected to Power Grids. *Energies* **2023**, *16*, 3678. [CrossRef]
11. Song, G.; Cao, B.; Chang, L. A Passive Islanding Detection Method for Distribution Power Systems with Multiple Inverters. *IEEE J. Emerg. Sel. Top. Power Electron.* **2022**, *10*, 5727–5737. [CrossRef]
12. Bansal, Y.; Sodhi, R. A Statistical Features Based Generic Passive Islanding Detection Scheme for IIDGs System. *IEEE Trans. Power Deliv.* **2022**, *37*, 3176–3188. [CrossRef]
13. Choudhury, B.K.; Jena, P. Superimposed Impedance-Based Passive Islanding Detection Scheme for DC Microgrids. *IEEE J. Emerg. Sel. Top. Power Electron.* **2022**, *10*, 469–483. [CrossRef]

14. Xia, Y.; Yu, F.; Xiong, X.; Huang, Q.; Zhou, Q. A novel microgrid islanding detection algorithm based on a multi-feature improved LSTM. *Energies* **2022**, *15*, 2810. [CrossRef]
15. Bakhshi, M.; Noroozian, R.; Gharehpetian, G.B. Novel Islanding Detection Method for Multiple DGs Based on Forced Helmholtz Oscillator. *IEEE Trans. Smart Grid* **2018**, *9*, 6448–6460. [CrossRef]
16. Dubey, A.K.; Kumar, A.; Mishra, J.P. Robust Adaptive Active Islanding Detection with α-Axis Disturbance Injection Under High Impedance Fault, Unbalanced Loading and Phase Failure in Grid Tied PV System. *IEEE J. Emerg. Sel. Top. Ind. Electron.* **2023**, *4*, 1213–1223. [CrossRef]
17. Dmitruk, K.; Sikorski, A. Implementation of the improved active frequency drift anti-islanding method into the three-phase AC/DC converter with the LCL grid filter. *Energies* **2022**, *15*, 1323. [CrossRef]
18. Gulipalli, S.C.; Chou, P.H.; Chen, Y.M.; Liu, T.I.; Chu, C.C. Frequency-Locked Loop Based New Automatic Phase-Shift Method for Active Islanding Detection of Three-Phase MicroGrid. *IEEE Trans. Ind. Appl.* **2023**, *59*, 5257–5268. [CrossRef]
19. Patekar, R.S.; Pal, D.; Panigrahi, B.K. Event-Triggered Hybrid Anti-Islanding Protection Scheme Based on Q-Axis Disturbance Injection. *IEEE Trans. Ind. Electron.* **2024**, *71*, 5787–5796. [CrossRef]
20. Gao, F.; Iravani, M.R. A Control Strategy for a Distributed Generation Unit in Grid-Connected and Autonomous Modes of Operation. *IEEE Trans. Power Deliv.* **2008**, *23*, 850–859.
21. Lasseter, R.H.; Chen, Z.; Pattabiraman, D. Grid-Forming Inverters: A Critical Asset for the Power Grid. *IEEE J. Emerg. Sel. Top. Power Electron.* **2020**, *8*, 925–935. [CrossRef]
22. Liu, Y.; Geng, J.; Xu, Y.; Zhang, H. A Novel Bearing Fault Detection by Primary Resonance of Saddle-Node Bifurcation Domains in a Hardening Duffing Oscillator. *IEEE Trans. Instrum. Meas.* **2024**, *73*, 1–11. [CrossRef]
23. Luo, W.; Cui, Y. Signal Denoising Based on Duffing Oscillators System. *IEEE Access* **2020**, *8*, 86554–86563. [CrossRef]
24. Pancóatl-Bortolotti, P.; Costa, A.; Enríquez-Caldera, R.; Guerrero-Castellanos, J.; Tello-Bello, M. Time-frequency high-resolution for weak signal detection using chaotic intermittence. *Digit. Signal Process.* **2023**, *141*, 104–160. [CrossRef]
25. Wang, Q.; Yang, Y.; Zhang, X. Weak signal detection based on Mathieu-Duffing oscillator with time-delay feedback and multiplicative noise. *Chaos Solitons Fractals* **2020**, *137*, 109832. [CrossRef]
26. Cao, S.; Li, H.; Zhang, K.; Yang, C.; Xiang, W.; Sun, F. A Novel Spiking Graph Attention Network for Intelligent Fault Diagnosis of Planetary Gearboxes. *IEEE Sens. J.* **2023**, *23*, 13140–13154. [CrossRef]
27. Vahedi, H.; Gharehpetian, G.B.; Karrari, M. Application of Duffing Oscillators for Passive Islanding Detection of Inverter-Based Distributed Generation Units. *IEEE Trans. Power Deliv.* **2012**, *27*, 1973–1983. [CrossRef]
28. Amini, H.; Mehrizi-Sani, A.; Liu, C.C. Substation Cyberattack Detection and Mitigation in a High-Noise Environment. In Proceedings of the IEEE Power & Energy Society Innovative Smart Grid Technologies Conference (ISGT), Washington, DC, USA, 19–22 February 2024.
29. Yousef, A.; Rida, S.; Ali, H.; Zaki, A. Stability, co-dimension two bifurcations and chaos control of a host-parasitoid model with mutual interference. *Chaos Solitons Fractals* **2023**, *166*, 112923. [CrossRef]
30. Piccirillo, V. L p optimal feedback control of homoclinic bifurcation in a forced Duffing oscillator. *Nonlinear Dyn.* **2023**, *111*, 13017–13037. [CrossRef]
31. Seyedi, M.; Taher, S.A.; Ganji, B.; Guerrero, J. A Hybrid Islanding Detection Method Based on the Rates of Changes in Voltage and Active Power for the Multi-Inverter Systems. *IEEE Trans. Smart Grid* **2021**, *12*, 2800–2811. [CrossRef]
32. Wang, G.; Chen, D.; Lin, J.; Chen, X. The application of chaotic oscillators to weak signal detection. *IEEE Trans. Ind. Electron.* **1999**, *46*, 440–444. [CrossRef]
33. Wang, G.; He, S. A quantitative study on detection and estimation of weak signals by using chaotic Duffing oscillators. *IEEE Trans. Circuits Syst. I* **2003**, *50*, 945–953. [CrossRef]
34. *Charge Controllers for Use in Photovoltaic Systems*; Underwriters Laboratories, Inc.: Northbrook, IL, USA, 2001.
35. Chaitanya, B.; Yadav, A.; Pazoki, M.; Abdelaziz, A.Y. A comprehensive review of islanding detection methods. In *Uncertainties in Modern Power Systems*; Academic Press: New York, NY, USA, 2021; pp. 211–256.
36. Ramachandradurai, S.; Krishnan, N.; Sharma, G.; Bokoro, P.N. Islanding Detection with Reduced Non-Detection Zones and Restoration by Reconfiguration. *Energies* **2023**, *16*, 3035. [CrossRef]
37. Resende, E.C.; Simoes, M.G.; Freitas, L.C.G. Anti-Islanding Techniques for Integration of Inverter-Based Distributed Energy Resources to the Electric Power System. *IEEE Access* **2024**, *12*, 17195–17230. [CrossRef]
38. Zeineldin, H.; El-Saadany, E.; Salama, M. Impact of DG interface control on islanding detection and nondetection zones. *IEEE Trans. Power Deliv.* **2006**, *21*, 1515–1523. [CrossRef]